

## The most sensitive initial error modes modulating intensities of CP- and EP- El Niño events

Qianqian Qi<sup>a,b</sup>, Wansuo Duan<sup>b,c,\*</sup>, Hui Xu<sup>b</sup>

<sup>a</sup> National Meteorological Center, China Meteorological Administration, Beijing 100081, China

<sup>b</sup> State Key Laboratory of Numerical Modeling for Atmospheric Sciences and Geophysical Fluid Dynamics (LASG), Institute of Atmospheric Physics, Chinese Academy of Sciences, Beijing 100029, China

<sup>c</sup> University of Chinese Academy of Sciences, Beijing 100049, China

### ARTICLE INFO

#### Keywords:

EP-El Niño events  
CP-El Niño events  
Spring predictability barrier  
Initial sea temperature errors  
The largest prediction errors

### ABSTRACT

The two types of El Niño events simulated by the Geophysical Fluid Dynamics Laboratory Climate Model version 2p1 (GFDL CM2p1) model and its “spring predictability barrier” (SPB) associations are examined. By conducting the ensemble hindcast experiments related to the sea temperature on the whole Pacific, both of the predictions for CP- and EP-El Niño show a significant SPB phenomenon, but the CP-El Niño features a much weaker SPB compared to the EP-El Niño. Further analyses revealed that, for CP-El Niño events, the initial sea temperature errors of the North Pacific with triple-like shape, referred to as negative Victoria Mode (VM) induces the largest prediction errors in Niño4 areas and modulates the intensities of CP-El Niño events. While for EP-El Niño events, the initial sea temperature errors in the subsurface layer of the western equatorial Pacific and the upper layer of the Southeast Pacific (15–30°S) with the meridional mode induce the largest prediction errors in Niño3 areas and modulates the intensities of EP-El Niño events. Obviously, results stress that, in order to reduce final prediction errors and obtain better predictions in terms of intensity on the two types of El Niño events, we should mainly focus on initial sea temperature accuracy in not only the subsurface layer of the west equatorial Pacific but also the surface layer of southeast Pacific and the region covered by the VM-like mode in the North Pacific.

### 1. Introduction

A number of studies have discussed the two types of inter-annual sea surface temperature (SST) variability in the tropical Pacific: the eastern Pacific El Niño (denoted as EP-El Niño) and the central Pacific El Niño (denoted as CP-El Niño) (Larkin and Harrison, 2005; Yu and Kao, 2007; Ashok et al., 2007; Kao and Yu, 2009; Kug et al., 2010). The EP-El Niño has its maximum SST anomalies (SSTA) warming centered in the eastern Pacific and the CP-El Niño has its maximum SSTA warming confined within the central Pacific (Kao and Yu, 2009; Kug et al., 2010; Weng et al., 2007). The two types of El Niño events have been suggested to produce various global climate anomalies in different regions, such as temperature anomalies and rainfall anomalies in Asia, Australia and North America (Weng et al., 2007; Yeh et al., 2009; Chen and Tam, 2010; Marathe et al., 2015; Yu et al., 2017; Chen et al., 2019). Studies on the

\* Corresponding author at: State Key Laboratory of Numerical Modeling for Atmospheric Sciences and Geophysical Fluid Dynamics (LASG), Institute of Atmospheric Physics, Chinese Academy of Sciences, Beijing 100029, China.

E-mail address: [duanws@lasg.iap.ac.cn](mailto:duanws@lasg.iap.ac.cn) (W. Duan).

<https://doi.org/10.1016/j.dynatmoce.2021.101257>

Received 10 March 2021; Received in revised form 2 August 2021; Accepted 7 September 2021

Available online 14 September 2021

0377-0265/© 2021 The Authors. Published by Elsevier B.V. This is an open access article under the CC BY-NC-ND license

(<http://creativecommons.org/licenses/by-nc-nd/4.0/>).

different impacts of CP- and EP- El Niño events on the global climate suggest that it is important to understand the predictability of each type of El Niño events, and to clarify the differences between the predictability dynamics of CP- and EP-El Niño events.

More studies revealed that, the different intensity of events could induce the natural disasters with different degrees for each type of El Niño events (Wu and Wu, 2018). For example, under the influence of the EP-El Niño events with medium and higher intensity, the onset date of the first rainy season in South China is earlier than normal while the ending date is later than normal and the duration is longer with higher than normal precipitation. The opposite is true when South China is under the influence of EP-El Niño events with weak intensity or under the influence of CP-El Niño events. In addition, some studies pointed out that, there exists strong relationship between the IOD and the intensity of El Niño events (Wang and Wang, 2014; He et al., 2015; Zhang et al., 2015; Fan et al. 2017). For example, IOD events often tend to occur during the strong EP-El Niño autumns, and the occurrence of IOD seem to be unrelated with the strength of CP-El Niño. These all imply that, the intensity predictions related to CP- and EP- El Niño events are of crucial importance to better study the relevant climate impacts.

Although the performance of climate models has been improved considerably, there still exists large intensity prediction uncertainty for EP- and CP-El Niño in most numerical models. For example, many ENSO prediction models predicted 2014 year into a moderate El Niño year while in fact the tropical Pacific only experienced a neutral conditions in 2014. In addition, the extremely strong 2015/16 El Niño event was forecasted to be a weak or slightly strong El Niño event (Ren et al., 2016). Kim et al., (2012b) found that the intensity prediction of CP-El Niño is weaker than observed with National Centers for Environmental Prediction (NCEP) Climate Forecast System (CFS) model. Zheng and Yu (2017) pointed out that, there exist larger systematic forecast biases for CP-El Niño prediction, and the ensemble prediction system developed at the Institute of Atmospheric Physics (IAP ENSO EPS) often predicted CP-El Niño into neutral climate phenomenon. Therefore, predicting the intensity of the two types of El Niño events accurately with ENSO prediction systems remains a challenge.

In the ENSO predictability, the “spring predictability barrier” (SPB) often cause large prediction errors at final prediction time. From the view of error growth, the so-called “spring predictability barrier” refers that, there often occurs a significant error growth during spring and/or summer when ENSO predictions are made before and throughout the spring (Webster and Yang, 1992; Lau and Yang, 1996; Mu et al., 2007a, 2007b). There are various hypotheses for the SPB. Some studies suggested that the air-sea coupling and oceanic thermocline-surface connection is the weakest during the spring season and SPB could be inherent feature of our climate system (Zhu et al., 2015). Some other studies pointed out that, the initial errors with the structure of a conditional nonlinear optimal perturbation (CNOP; Mu et al., 2003) cause the most prominent SPB (Duan et al., 2009; Yu et al., 2009; Duan and Wei, 2012; Duan and Hu, 2016). Considering that CP-El Niño presents different features from EP-El Niño events, therefore, recent studies have discussed the SPB phenomenon related to CP-El Niño events. Using the Zebiak-Cane model (Zebiak and Cane, 1987) corrected by the optimal forcing vector (OFV) approach (Duan et al., 2014), Tian and Duan (2015, 2016) concluded that, there also exists the SPB phenomenon for CP-El Niño prediction. More recently, Hou et al. (2019) revealed that, the summer PB often occurs in the CP-El Niño events with the monthly mean data of six coupled models pre-selected from CMIP5. In any case, all these studies imply that CP-El Niño event forecast also shows a season-dependent predictability barrier.

Recently, more and more studies have emphasized the role of subtropical Pacific in the two types of El Niño onset and prediction, especially the CP-El Niño events. Yu et al. (2010) pointed out that, the air-sea interaction in the subtropical North Pacific may play an important role for the initiation of CP-El Niño. Ding et al. (2015) discussed that, the quadrupole SST variability in the subtropical South Pacific have a different and relatively independent influence on ENSO prediction compared with the extratropical North Pacific. Yeh et al. (2015) discussed the relationship between the North Pacific climate variability and CP- El Niño events. Furthermore, Zhu et al. (2016) pointed out that, the meridional mode structure in the subtropical Pacific is usually not well captured by contemporary forecast systems and could result in significant ENSO false alarms. Min et al. (2017) revealed that the Meridional Mode structure in the South Pacific mainly favors the development of SSTAs in the eastern equatorial Pacific, whereas the Meridional Mode in the North Pacific mainly contributes to the development of SSTAs in the central equatorial Pacific. More recently, Wang et al. (2019a) evaluated the relationship between the frequency of CP- El Niño and North Pacific Oscillation (NPO) using the 25 CMIP5 models. Wang et al. (2019b) stressed the roles of tropical and subtropical wind stress anomalies in the CP- El Niño onset. Hou et al. (2019) identified the initial errors that often induce season-dependent PB for CP- and EP-El Niño events based on multi-model outputs data, and their results indicated that the specific structures in the North Pacific and Southeast Pacific may play an important role in El Niño predictions.

As we all know, although most climate models can successfully predicted the onset of the El Niño events, they often cannot predict the intensity of the events exactly. That's, there exist large prediction errors related to the intensity prediction of CP- and EP- El Niño events. Naturally, several questions are thus raised: When we integrate the numerical model by conducting the ensemble hindcast experiments related to the sea temperature on the whole Pacific, what kind of initial errors on the whole Pacific cause the significant SPB, especially the largest prediction errors for CP- and EP-El Niño? Specifically, what's the most sensitive initial error modes modulating intensities related to CP- and EP-El Niño? Furthermore, if additional observations are developed in these areas and then assimilated to numerical models, whether or not the large prediction errors of CP- and EP- El Niño may be reduced and even to be avoided?

In this paper, we use a complex global air-sea coupling model to explore the initial errors on the whole Pacific that result in the largest prediction errors for the two types of El Niño. The remainder of this paper is organized as follows: in Sect. 2, the model and its experimental strategy used in this paper are introduced. In Sect. 3, the SPB phenomenon related to EP- and CP- El Niño events are investigated. In Sect. 4, the initial errors that induce a significant SPB, especially the largest prediction errors of corresponding Niño areas for the two types of El Niño events and their seasonal growth mechanisms are explored. In Sect. 5, by conducting a series of sensitive tests, we identify the most sensitive initial error modes modulating intensities related to CP- and EP- El Niño events. And then in Section 6, we summarize the whole study and offer further discussion.

## 2. Model and experimental strategy

### 2.1. GFDL CM2p1 model and its main inter-annual variance character

In this study, we will use Geophysical Fluid Dynamic Laboratory (GFDL) CM2p1 coupled model. The GFDL CM2p1 contains four components with the ocean, atmosphere, land and sea ice modules and it is a globally fully-coupled model. Ocean's hydrostatic primitive equations is used as a numerical representation in the ocean component of GFDL CM2p1. The resolution of the ocean component is  $1^\circ \times 1^\circ$  in most ocean regions, and the meridional resolution is encrypted to  $1/3^\circ$  near the equator. There are 50 vertical levels, with a 10 m resolution in the upper 225 m. The atmospheric component in GFDL CM2p1 is AM2p12b and its horizontal resolution is  $2^\circ$  (latitude)  $\times$   $2.5^\circ$  (longitude) with 24 vertical levels. The land module uses Land Dynamics model version 2.1 (LM2.1; Milly and Shmakin, 2002) and the sea ice module uses GFDL Sea Ice Simulator (SIS; Delworth et al., 2006). All the four modules in GFDL CM2p1 exchange fluxes every 2 h through the GFDL's Flexible Modeling System (FMS, <http://www.gfdl.noaa.gov/fms>). More details related to GFDL CM2p1 can be found in Delworth et al. (2006) and Griffies (2009).

We use the land cover, tracer gases, aerosols, and insolation during the year 1990 to force the GFDL CM2p1 model and integrate the model for 300 years. The last 250 years are analyzed in order to eliminate the impact of initial adjustment processes. Fig. 1 presents the standard deviation of the simulated and observed inter-annual SST anomalies (SSTA) in November–January (NDJ) over the tropical Pacific. It is found that the spatial pattern of the inter-annual variability strongly resembled the mature phase mode of ENSO, and the simulated results are comparable to those in observation except that the area of strong variability simply expands westward substantially and the belt of the strong SSTA variability is more confined within the equatorial zone in the model than in observations, which may be a common symptom in the current coupled global climate models (CGCMs) (AchutaRao and Sperber, 2002; Bellenger et al., 2014; Ham and Kug, 2012; Lin et al., 2015; Wang et al., 2021).

Furthermore, the first two leading EOF modes of the monthly SSTA over the tropical Pacific region are presented in Fig. 2. The structure of EOF1 is similar to EP-El Niño pattern [Rasmusson and Carpenter, 1982] and EOF1 mode explains about 55.7% of the tropical Pacific SST variability for the integrate period of 300 years. The EOF2 mode explains 9.3% of the SST variability and it possess a zonal tripole pattern in the tropical region and resembles the CP-El Niño pattern. We also find that, the magnitudes of PC1 and PC2 are comparable and PCs of these two EOFs present the different time scales. Concretely, the PCs of EOF1 mainly present the interannual timescale, while the PCs of EOF2 mainly present the decadal variance and show the quite small interannual timescale. By analyzing the power spectra of PC1 and PC2 corresponding to EOF1 and EOF2 mode respectively, we find that, there only exists the interannual timescale variance (around 4 years) for the PC1 indices; the PC2 indices display a major peak at a decadal timescale (around 15 years) and the interannual timescale variance (around 4 years). This is at odds with the Nino 3 index that shows comparable peak variances at period of about 3–5 years and Nino 4 index that shows comparable peak variances at period of about 4 and 10 years. The results are consistent with the studies of Sullivan et al. (2016). Therefore, these two modes of EOF1 and EOF2 may represent EP- and CP-El Niño pattern. Also, it is reasonable to point out that, the coupled model GFDL CM2p1 has the ability to replicate the EP- and CP-El Niño

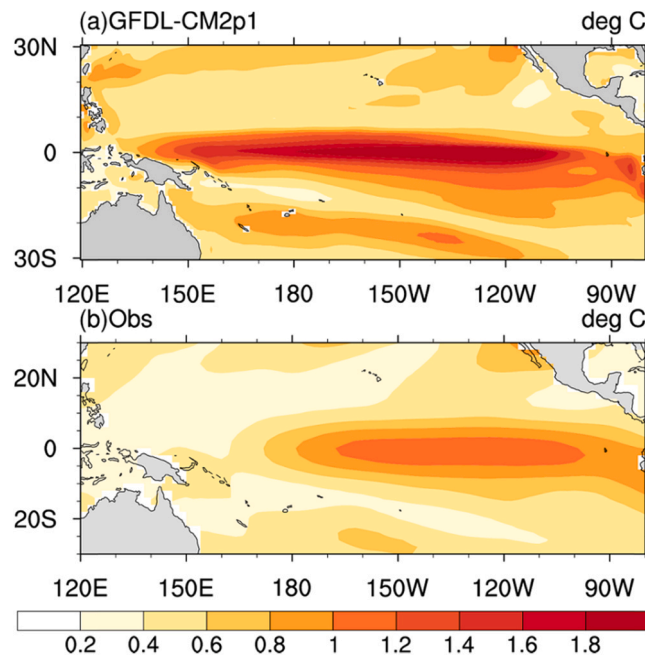


**Fig. 1.** The standard deviation of SST ( $^\circ\text{C}$ ) over the tropical Pacific during NDJ from (a) the model GFDL-CM2p1 of 250 years' control test datas and (b) the monthly Extended Reconstructed Sea Surface Temperature Version 4 (ERSST V4) dataset during the period 1951–2015.

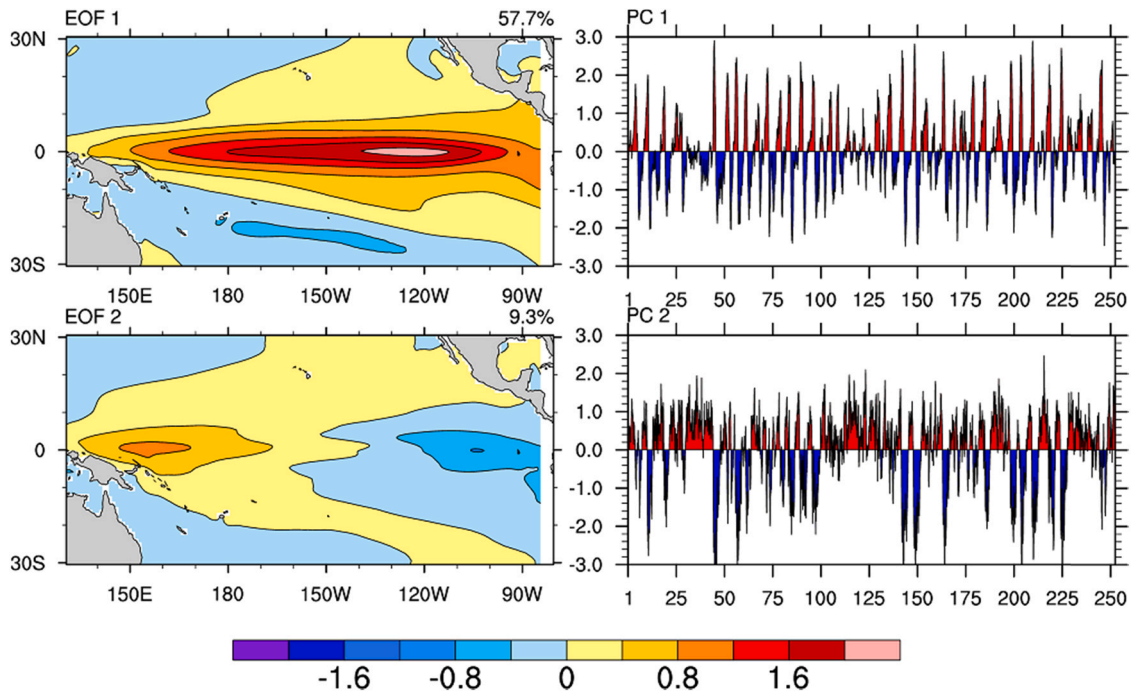


Fig. 2. The top two EOF modes and the corresponding time series of tropical Pacific SSTA deviations of the principal components from the GFDL-CM2p1 model.

events.

In addition, after removing the ENSO influences on the whole Pacific, the SST anomaly of the leading mode in the North Pacific and the South Pacific are shown in Fig. 3. Compared with observation, the first mode of the North Pacific SST anomaly closely resembles the pattern with the Vectoria mode (VM) of Bond et al. (2003), while the first mode of the South Pacific SST anomaly are closely similar to the South Pacific Meridional Mode (SPMM) introduced by Zhang et al. (2014a, b). The results show that, the GFDL CM2p1 coupled model can capture the SST anomaly signals related to the North Pacific and the South Pacific. As such, it is reasonable to investigate the predictability for El Niño events on the whole Pacific with GFDL CM2p1 coupled model.

2.2. Experimental strategy

Firstly, we select eight EP- and CP- El Niño events from the control simulation respectively. For discussion purpose, we simply define Year (0) as the year of El Niño growth and Year (1) as the year of El Niño decay while Year (-1) is the year preceding Year (0). Fig. 4 presents the evolution of Niño index related to EP- and CP- El Niño events respectively. The eight EP-El Niño events and eight CP-El Niño events all tend to onset in boreal spring or early summer and peak in late autumn or winter of Year (0), then decay gradually in the Spring or Summer of Year (1). As such, the two types of El Niño events present the obvious phase locking features. In addition, the

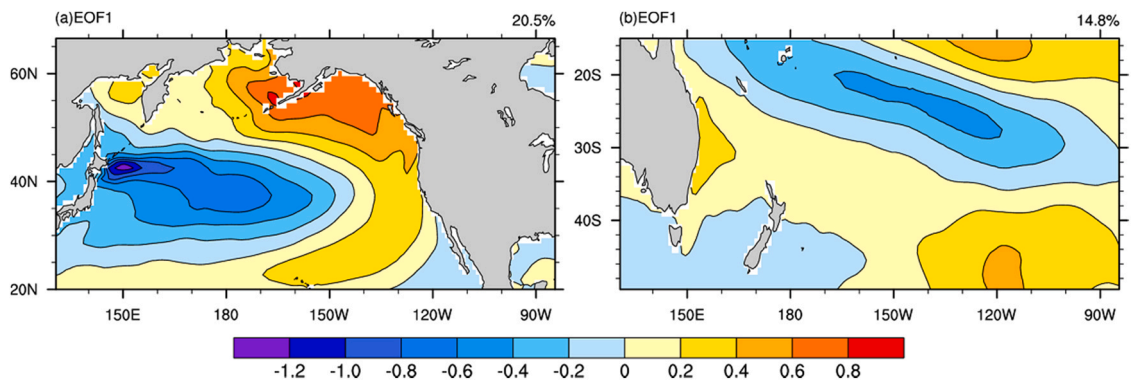
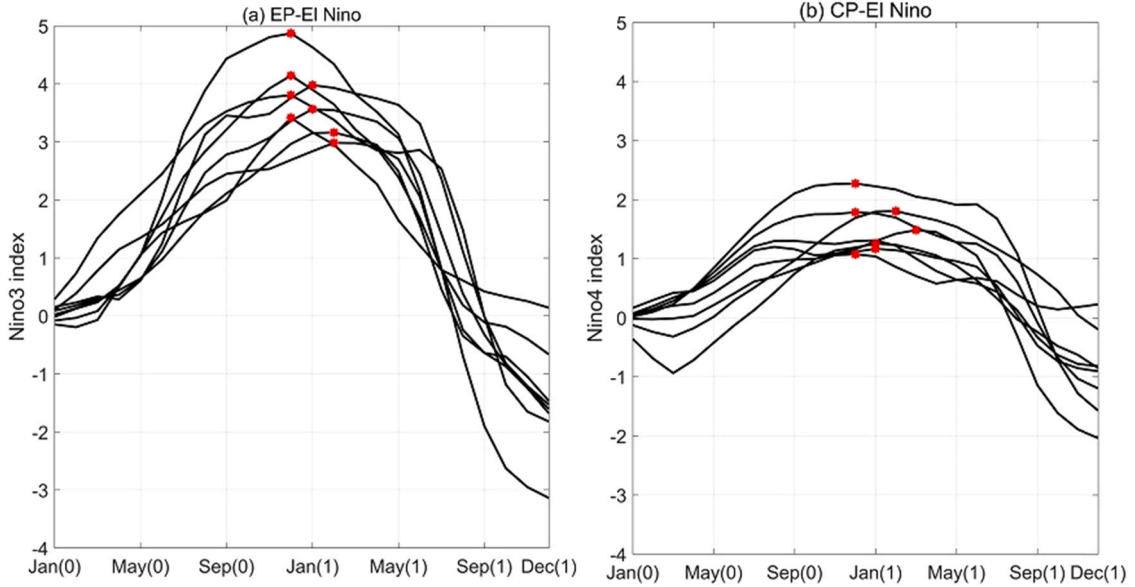


Fig. 3. The first EOF mode of subtropical Pacific SSTA deviations of the principal components from the GFDL-CM2p1 model for (a) the subtropical of North Pacific and (b) the subtropical of South Pacific.



**Fig. 4.** The evolution related to Niño index of EP-El Niño events and CP-El Niño events derived from GFDL-CM2p1 model with (a) the Niño3 index and (b) the Niño4 index. The red star indicate the month of the year when the Niño index reaches the peak. In the x-axis, Month (0) is denoted as the month of El Niño attaining peak year and Month (1) represents the month of decaying the El Niño year.

amplitude of Niño 3 index related to EP-El Niño events is significantly larger than the amplitude of Niño 4 index related to CP-El Niño events. The peak of the former is about twice that of the latter and the intensity ratio related to EP-El Niño events and CP-El Niño events agrees with the observation features.

With the selected CP- and EP- El Niño events, we conduct perfect model experiments to investigate the effects of initial errors on the two types of El Niño events prediction uncertainties. In this study, the GFDL CM2p1 coupled model is supposed to be perfect and the prediction uncertainties of the two types of El Niño events are considered to be caused only by initial errors. Since the model is assumed to be perfect, the two types of El Niño events generated by the model’s control run are regarded as the “true state” El Niño events to be predicted. It has been noticed that the EP- and CP- El Niño events selected from the model’s control run are often strong, which may be caused by the forcing process in the integrated simulation. The initial errors are imposed on the initial sea temperature for the selected eight “true state” EP-El Niño events and eight “true state” CP-El Niño events. By taking the differences between the Pacific sea temperature of the “true state” El Niño events at the start month and that in each month of the 4 years (a total of 48 months) preceding the start month, we obtain the initial errors sample set. Thus, there are a total of 48 initial errors for one start month with each event. As is known that, the cycles related to the two types of El Niño events are approximately 4 years respectively in the GFDL CM2p1 coupled model, so the patterns of sea temperature anomalies within 4 years may represent much ergodic initial errors. In our studies, we found that the initial errors being normalized often cause an initial shock phenomenon that characterized as a rapid growth of errors within a short time after the beginning the predictions, which may be due to the dynamical unbalance among different levels of the upper ocean temperature field induced by normalized initial errors. It is therefore pointed out that the magnitudes of the initial errors are not constrained uniformly in our numerical experiments and the spatial pattern of initial errors is mainly emphasized.

With these initial errors, leading 12-month predictions are made on the start month being October (−1) and January (0) for each El Niño events. Clearly, the above predictions with the selected start months are just across the growth phase of the El Niño events and pass through the spring. In total, there are 768 predictions for each type of El Niño events. For these predictions, the initial errors of the sea temperature cover the Pacific region (130° E–85° W, 66.5° S–66.5° N) from the surface to a 165 m depth. Therefore, in this study, we will study how the initial sea temperatures uncertainties over the whole Pacific impact the predictability of the two types of El Niño events.

The prediction errors are calculated by taking the difference between the SSTA of the predicted El Niño events and those of the “true state” El Niño events, which can be defined in Eq. (1):

$$T'(t) = \|T^p(t) - T^t(t)\| = \sqrt{\sum_{ij} [T^p_{ij}(t) - T^t_{ij}(t)]^2}, \tag{1}$$

where the  $T^p$  and  $T^t$  are the predicted SST and the “true” SST, respectively, at lead time  $t$ , and  $T'(t)$  is the prediction error induced by the initial errors.  $(i, j)$  represents the grid points of the equatorial Pacific region (20° S–20° N, 130° E–85° W). Then, the growth tendency  $k$  of the prediction errors at each season can be approximately calculated by

$$k \approx \frac{T'(t_2) - T'(t_1)}{t_2 - t_1}, \tag{2}$$

where  $T'(t_1)$  and  $T'(t_2)$  denote the prediction errors at  $t_1$  and  $t_2$  respectively; the future times  $t_1$  and  $t_2$  represent the beginning and the end time of the given prediction period. A positive (negative)  $k$  value indicates an increase (decrease) in error, and the greater the absolute value of  $k$  is, the faster the increase (decrease) in error becomes.

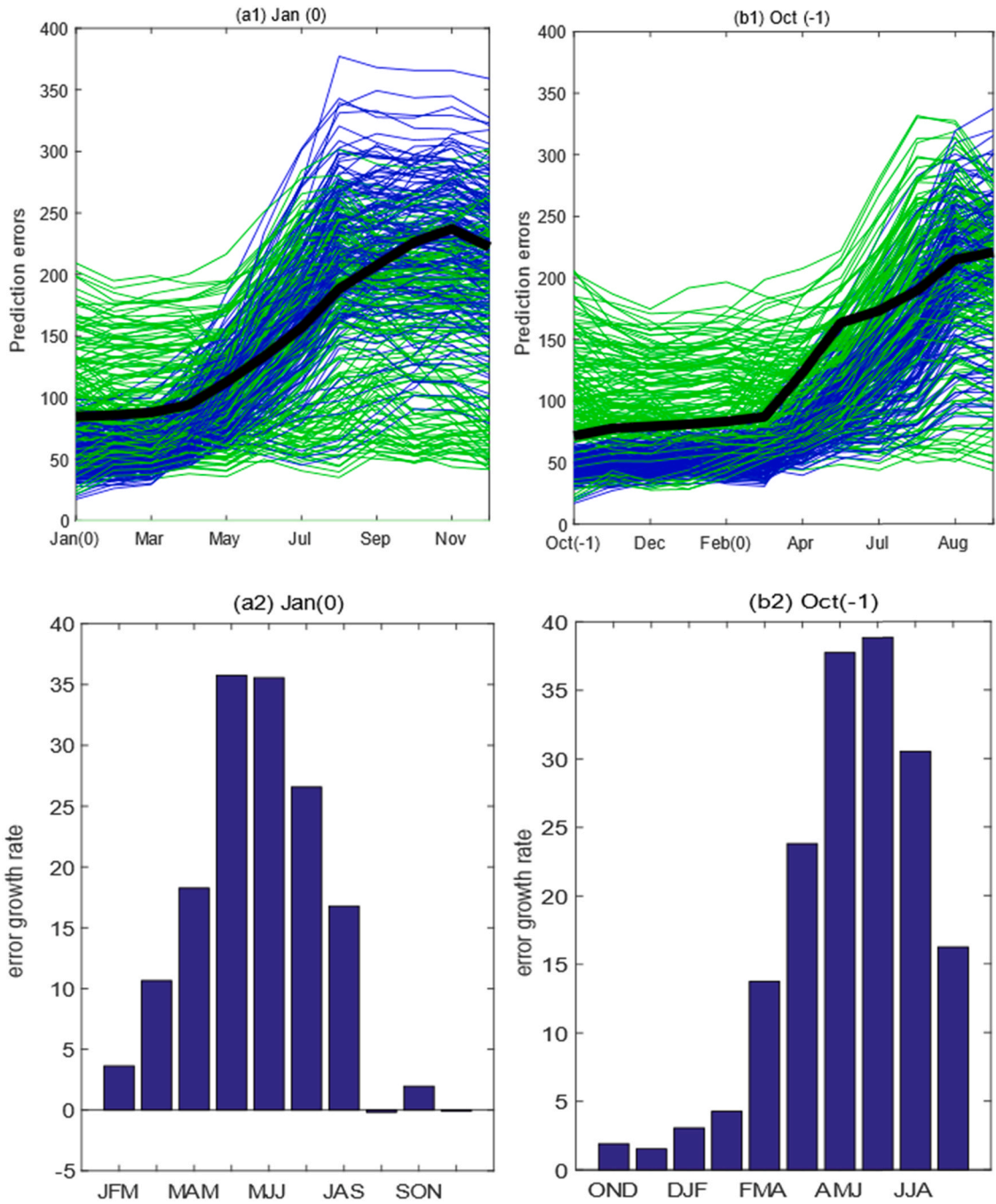


**Fig. 5.** For EP-El Niño events, (a1) and (b1) represent the evolution of the prediction errors (color curves) for ensemble forecast members with start months Jan (0) and Oct (-1) respectively. The black curves represent the means of the prediction errors of the ensemble forecast members. (a2) and (b2) represent the seasonal error growth tendencies of the ensemble-mean forecast (blue bar) with start months Jan (0) and Oct (-1) respectively.

### 3. the SPB phenomenon related to EP- and CP- El Niño events

As described in the introduction, the so-called SPB refer to that ENSO predictions systems encounter a season-dependent predictability barrier and then induce a large prediction error at further certain time. From the view of error growth, when the 12-month leading prediction possess a large prediction error at the final prediction time and has the significant error growth during spring and/or the beginning of summer, we think that there occurs the so-called SPB for this prediction. With the character of SPB, we firstly calculated the prediction errors of SSTA at the end of prediction time and the relevant seasonal growth tendency based on formula (1)

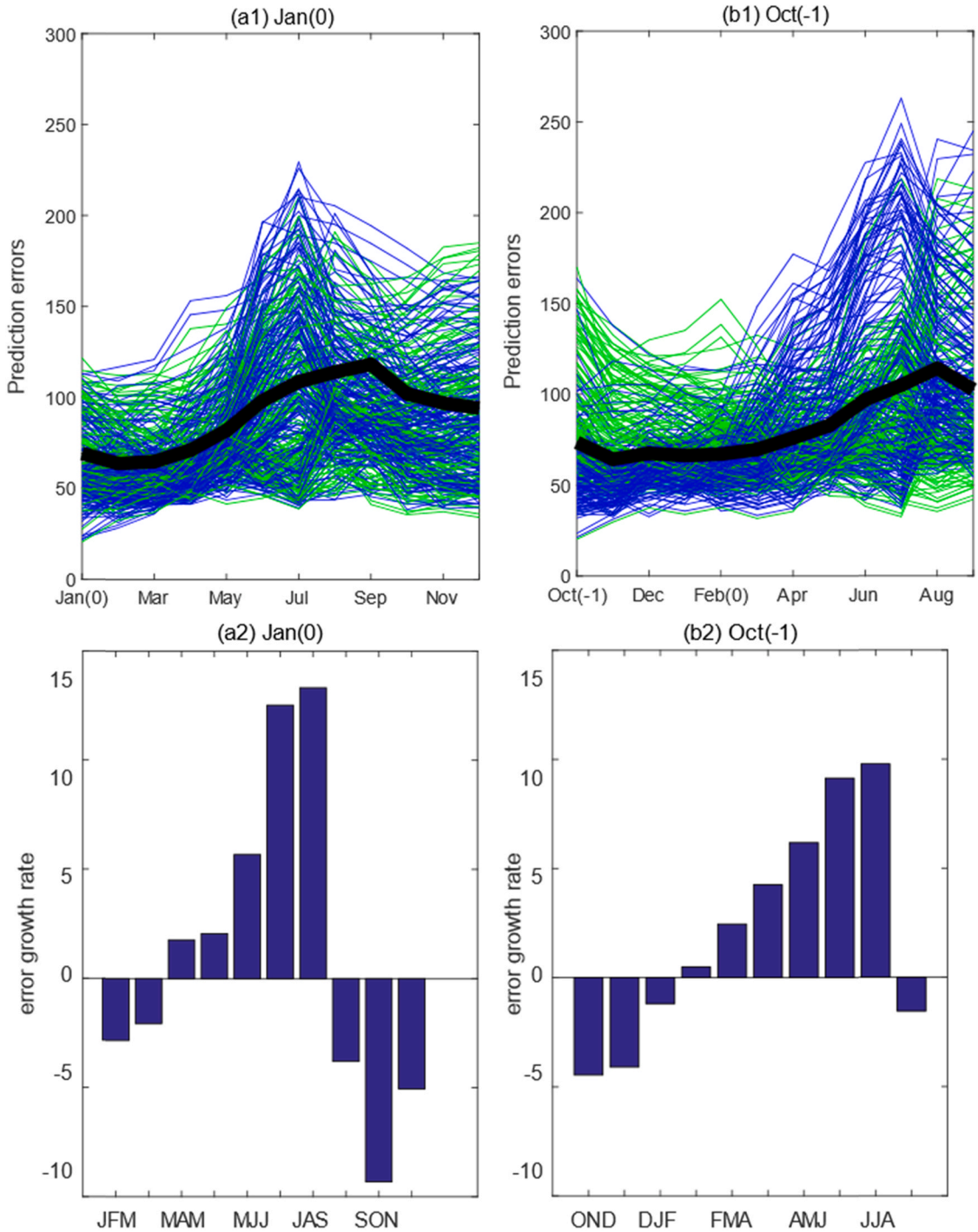


Fig. 6. As in Fig. 5, but for CP-El Niño events.

and (2). Then, according to the occurring conditions of SPB, we identify 415 predictions [201 for the start month October (-1) and 214 for January (0)] that yield a significant SPB from the 768 predictions for eight EP-El Niño events. To address the SPB phenomenon for the whole EP-El Niño events, we then evaluate the evolution of the SSTA prediction errors for each ensemble forecast members and estimate its seasonal growth tendency of the ensemble-mean forecasts (Fig. 5). The figure shows that the prediction errors tend to experience their largest growth rate in spring (AMJ and/or MJJ) and exhibit a significant season-dependent evolution.

For eight CP-El Niño events, we also identify 292 predictions [164 for the start month October (-1) and 128 for January (0)] that make a significant contribution to a prominent SPB from the 768 predictions. We present in Fig. 6 the evolution of the prediction errors and the ensemble mean of their seasonal growth tendency corresponding to the initial errors of CP-El Niño events. It is illustrated that, the initial errors exhibit significant season-dependent evolution for both start months and their largest growth tendency tends to be in the JJA and/or JAS season.

Therefore, for both the EP- and CP- El Niño events, the results indicated that the prediction errors tend to experience their largest growth rate in spring and/or summer and exhibit a significant season-dependent evolution, generating a significant SPB. However, compared with the EP-El Niño events, the relevant seasonal growth tendency level in late spring or early summer is much weaker for the CP-El Niño events; the prediction errors related to the CP-El Niño events at the end of the 12-month lead time are much smaller; the

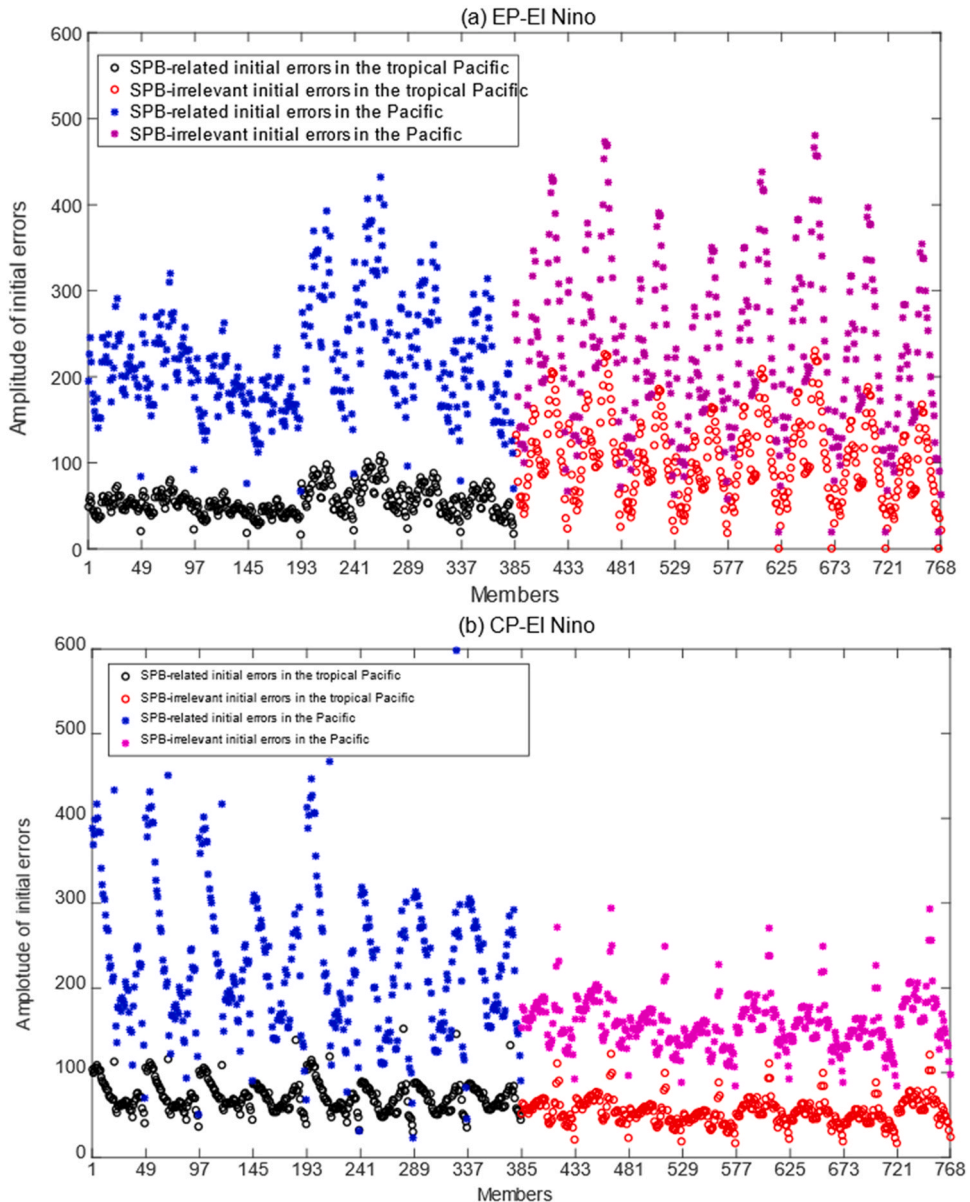
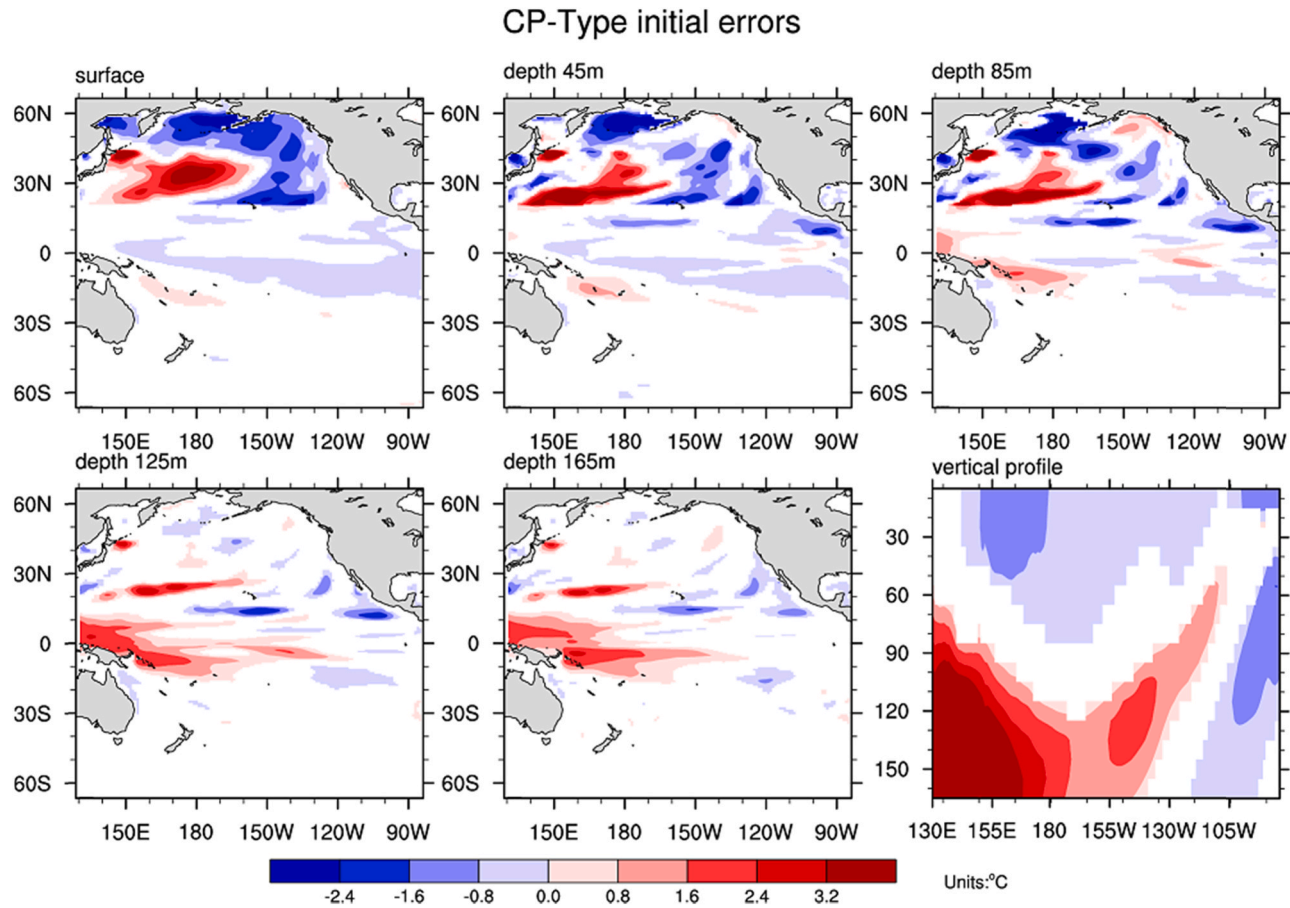


Fig. 7. the amplitude scatter diagram of SPB-related and SPB-irrelevant initial errors in the tropical Pacific and Pacific respectively.



**Fig. 8.** Composite of anomalous sea temperature (units: °C) of the CP-type initial errors that induce a significant SPB especially the largest prediction errors in Niño4 areas. The top 5 images correspond different ocean depths, as from the sea surface to 45 m, then to 85 m, 125 m and 165 m. The last one is the meridional mean of the sea temperature anomaly over 5°S–5°N. Composites of initial errors not exceeding the 95% significance level are masked.

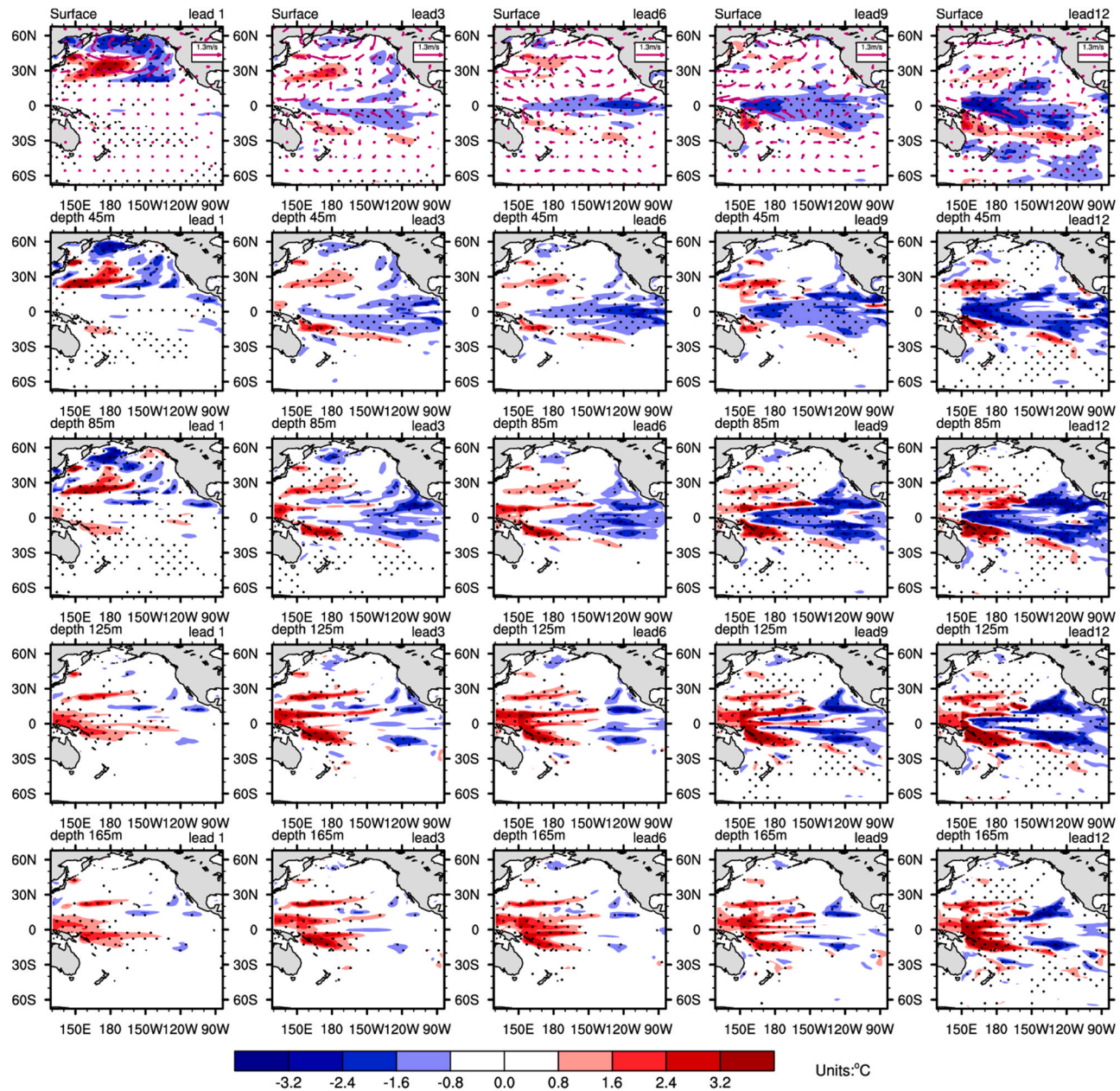


Fig. 9. Composite of the evolutions of anomalous sea temperature (units: °C) and horizontal wind (units: m/s) of CP-type initial errors as shown with lead 1, lead 3, lead 6, lead 9 and lead 12 months predictions. The dotted areas denote those exceeding the 95% significance level. The rows correspond to sea depths, as from the sea surface to 5 m, then to 45 m, 85 m, 125 m and 165 m.

prediction members in CP-El Niño events which make a significant contribution to the SPB are less than that in EP-El Niño events. So, although there occurs the SPB phenomenon for the two types of El Niño events, there occurs the much weaker SPB phenomenon for CP-El Niño events.

In order to address the SPB phenomenon, Figs. 5(a1) (b1) and 6 (a1) (b1) only present the error evolution of the tropical Pacific covering region ( $20^{\circ}$  S– $20^{\circ}$  N,  $130^{\circ}$  E– $85^{\circ}$  W). In fact, our initial errors are constructed covering the whole Pacific region ( $130^{\circ}$  E– $85^{\circ}$  W,  $66.5^{\circ}$  S– $66.5^{\circ}$  N) from the surface to a 165 m depth. From these two figures, we notice that most of these strong SPB cases are associated with small initial errors (blue curves). On the other hand, many of the cases presumably without SPB show very large initial errors (green curves). Although these strong SPB cases are actually associated with small initial errors in tropical Pacific, the initial error in the whole Pacific region are not always small when occurring the SPB. That's to say, the initial errors in the extratropical Pacific and the subsurface ocean temp may be large and play an important role in contributing to the occurrence of SPB. In order to illustrate it, we calculate the magnitude of initial errors covering the tropical Pacific and the whole Pacific respectively when occurring the SPB and no-SPB respectively (see Fig. 7). From the scatter diagram, we can see that, the mean amplitude of SPB-related initial errors in the tropical Pacific are often smaller than that for the SPB-irrelevant initial errors. However, the mean amplitude of SPB-related initial errors in the whole Pacific are often larger than that for the SPB-irrelevant initial errors. The results imply that, the initial errors in the ex-tropical Pacific may play an important role in contributing to the occurrence of SPB.

#### 4. The most sensitive initial errors and their related error growth

As mentioned in Section 3, both the predictions related to the two types of El Niño events encounter the SPB phenomenon. Previous studies have shown that the initial errors with the particular structures could induce the SPB. Related to EP-El Niño events, the CNOP-type initial errors have been explored by tracing the growth of the optimal initial error of Zebiak-Cane model (Yu et al. 2009; Duan et al. 2009) and the Community Earth System Model (CESM) (Duan and Hu, 2016). Related to CP-El Niño events, Tian and Duan (2015) apply the OFV approach to the Zebiak-Cane model and simulated several EP- and CP- El Niño events. Their results show that, for the CP-El Niño events, one type of CNOP-type errors possessing a sea surface temperature anomaly (SSTA) pattern with negative anomalies in the equatorial central western Pacific, positive anomalies in the equatorial eastern Pacific, and accompanied by a thermocline depth anomaly pattern with positive anomalies along the equator can induce the significant SPB. However, previous studies only focus on the tropical Pacific and ignore the impact of Subtropical Pacific on the two types of El Niño events. In this section, when concerning about the whole Pacific, we try to answer that which features of the initial errors induce the largest prediction errors for each type of El Niño events. Furthermore, how do these initial errors evolve and module the intensities of CP- and EP- El Niño predictions?

##### 4.1. The initial errors that induce the most significant SPB for CP-El Niño events and its related initial error growth

In Section 3, for CP-El Niño events, we have identified 292 predictions that yield a significant SPB. In order to obtain the features of initial errors that induce a significant SPB especially the largest prediction errors in Niño4 areas, firstly, we selected 149 predictions which have larger prediction errors in Niño4 areas from the above 292 predictions; and then we perform the Combined Empirical Orthogonal Function (CEOF) analysis for these 149 initial errors and take the top three EOF modes which account for the 55% of the total variance. The top three EOF modes and their opposite modes may represent the dominant spatial characteristic of the initial errors that often cause a significant SPB. We denote these six modes as EOF\_1 +, EOF\_1-, EOF\_2 +, EOF\_2-, EOF\_3 +, EOF\_3-, respectively. Since we try to find the domain mode of the initial errors that induce the largest prediction errors, we therefore firstly select the members whose initial errors are highly correlated (including positively and negatively correlated) with EOF\_1 +, EOF\_2 +, EOF\_3 +, respectively. It should be noticed that, the correlations are referred to spatial correlation in our calculations. Then, for the members that are highly positively or negatively correlated with EOF\_1 +, EOF\_2 +, and EOF\_3 +, we calculate the prediction errors respectively for SSTA over the Niño4 areas at the end of the 12-month lead time based on Eq. (1). By comparing prediction errors corresponding to different groups, results imply that the prediction errors induced by the forecast members whose initial errors are of the EOF\_1- modes are the largest ones. Following this, we composite the initial errors corresponding to the EOF\_1- mode and obtain the spatial pattern of initial errors which induce the significant SPB, especially the largest prediction errors at the end of 12-month lead time. We denoted the above pattern as the CP-Type initial errors.

Fig. 8 present the structures of CP-Type initial ocean temperatures at different depth. It is shown that the CP-Type initial errors exhibit the strong anomalies over north Pacific upper layers with a triple-like shape, referred to as negative Victoria Mode (VM-), and the subsurface temperature anomaly with positive anomalies in the lower layers of the western equatorial Pacific. Having obtained the CP-Type initial errors which induce the significant SPB, especially the largest prediction errors in Niño4 areas, we then integrate the GFDL-CM2p1 model for 1 year with the initial fields being the initial sea temperature of each “true state” CP-El Niño event plus CP-Type initial errors; and then, by subtracting the “true state”, there obtained the evolution of prediction errors caused by CP-Type errors for CP-El Niño events (see Fig. 9). By analyzing the evolution patterns of prediction errors including the whole Pacific SSTA, sea surface wind anomaly and equatorial subsurface temperature anomaly components, we find that, in the tropics, the CP-Type initial errors often evolve from a neutral state to a La Nina-like mode, finally triggering a cold bias of prediction especially at Niño 4 area at leading 12 months. Fig. 9 implies that, the positive subsurface temperature anomaly in the greater depths of the western equatorial Pacific in above CP-Type initial errors doesn't have a development over a long period of time and these indicate that it could not be the final source of prediction errors. So, what kind of physical process causes the sustainable development of the negative SSTA error in the central equatorial Pacific?

In fact, the initial ocean temperature errors in the subtropical North Pacific of the VM-like component of CP-Type initial errors

### EP-Type initial errors

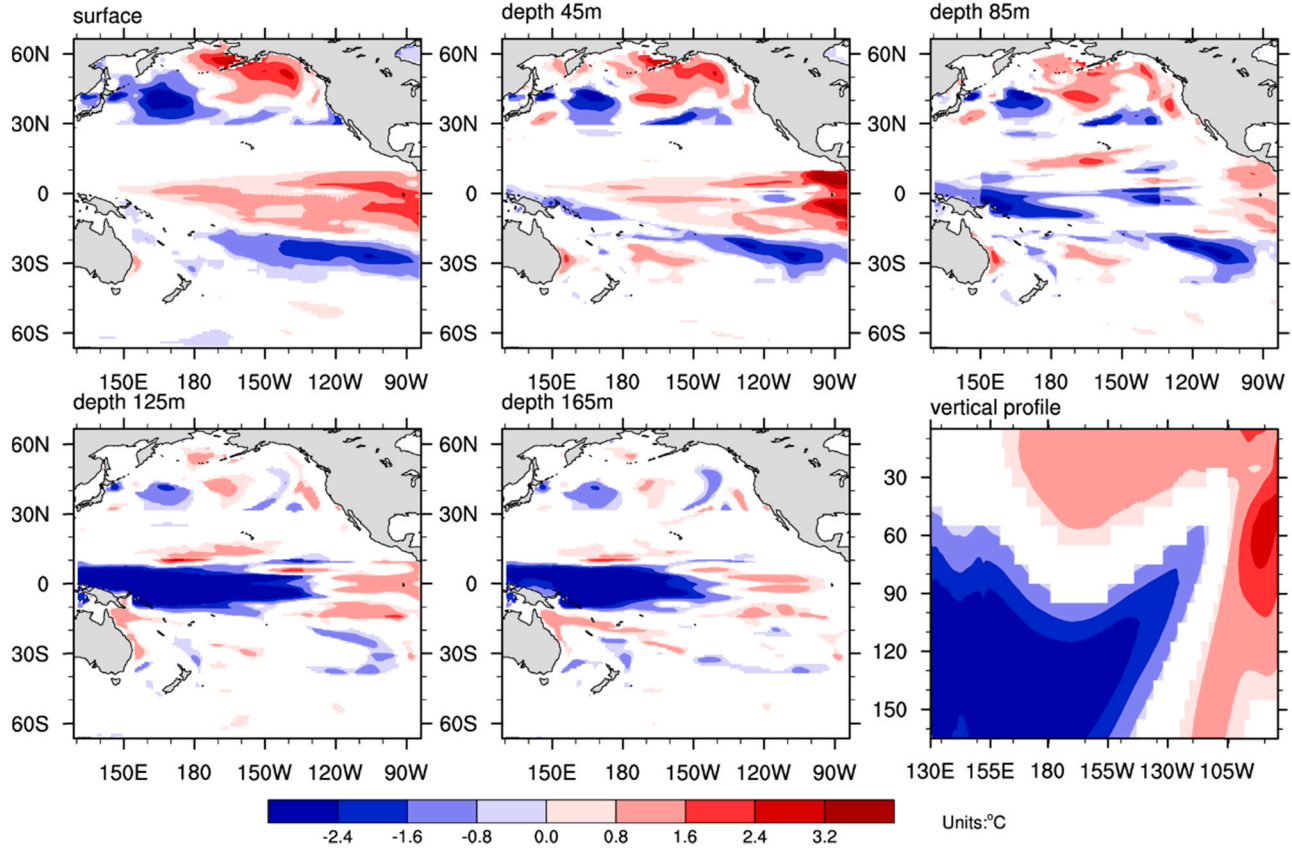


Fig. 10. As in Fig. 8, but for the EP-Type initial errors.

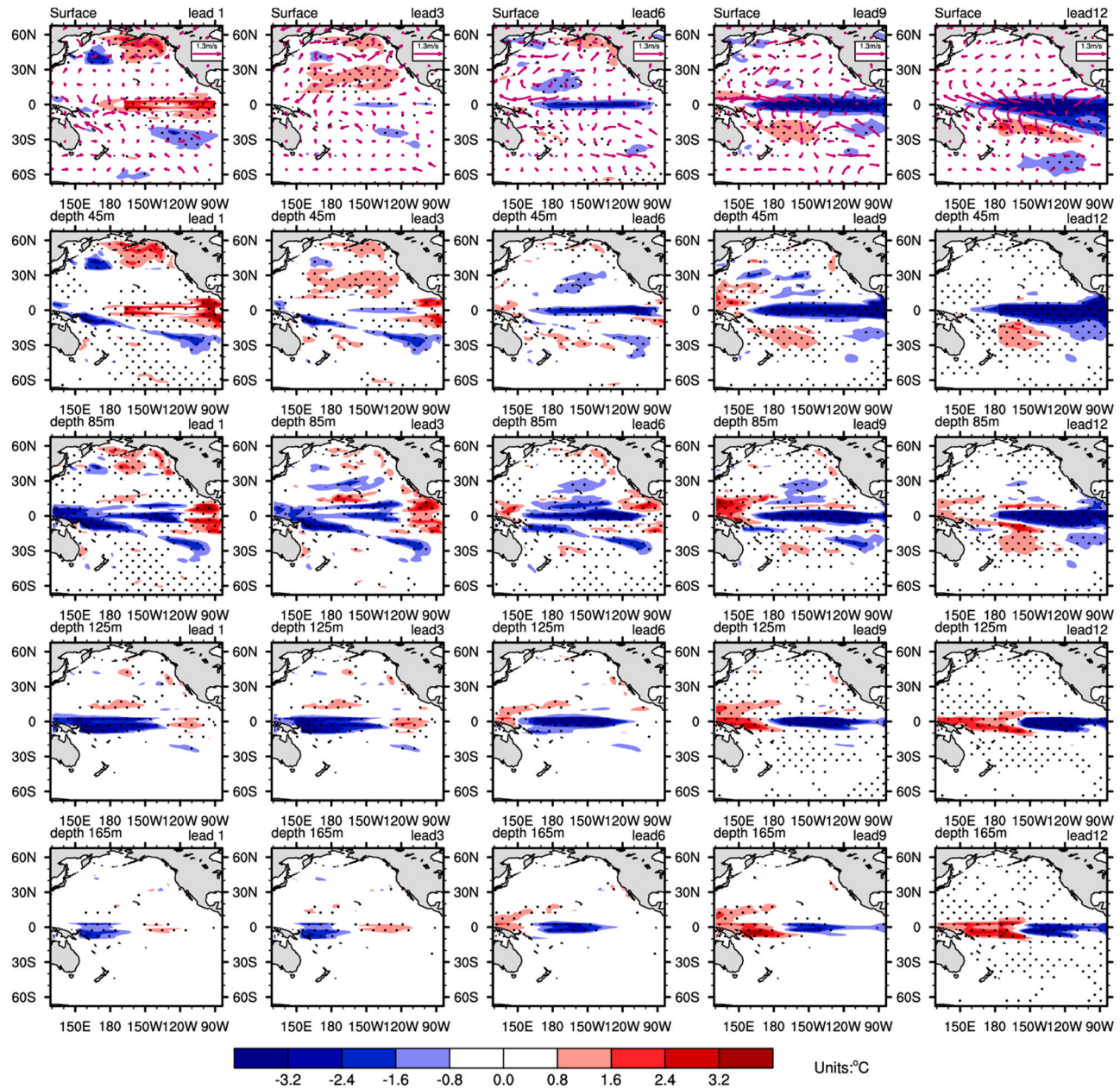


Fig. 11. As in Fig. 9, but for the EP-Type errors.

firstly induce the abnormal air convection and then cause the atmospheric baroclinic response. This will change the sea surface wind over the North Pacific. At the same time, the abnormal northeast wind errors in the subtropical North Pacific are established and spread to the equatorial Pacific gradually. During the air-sea interaction process, the cold SST footprints propagate to the equatorial Pacific gradually and trigger the abnormal easterly wind in the equatorial Pacific, which will enhance the negative SSTA errors and propagate westwards to the central Pacific. Therefore, the ocean temperature errors with the structure of north Pacific VM- induce the development and the mature of negative SSTA errors in the equatorial Pacific especially at Niño 4 areas, which causes the under-predictions of the CP-El Niño events in terms of intensities.

#### 4.2. The initial errors that induce the most significant SPB for EP-El Niño events and its related initial error growth

As demonstrated in Section 3, for EP-El Niño events, we have identified 415 predictions that yield a significant SPB. In order to obtain the features of initial errors that induce a significant SPB especially the largest prediction errors in Niño 3 areas, Similarly to that performed for the CP-El Niño events, firstly, we selected 215 predictions which have larger prediction errors in Niño3 areas from the above 415 predictions; and then we perform the Combined Empirical Orthogonal Function (CEOF) analysis for these 215 initial errors and take the top three EOF modes which account for the 67% of the total variance. We denote these six modes as EOF\_1 +, EOF\_1-, EOF\_2 +, EOF\_2-, EOF\_3 +, EOF\_3-, respectively. Since we try to find the domain mode of the initial errors that induce the largest prediction errors in Niño 3 areas, we therefore select the members whose initial errors are highly correlated (including positively and negatively correlated) with EOF\_1 +, EOF\_2 +, EOF\_3 +, respectively. For the members that are highly positively or negatively correlated with EOF\_1 +, EOF\_2 +, and EOF\_3 +, we calculate the Niño 3 SSTA prediction errors at the end of the 12-month lead time. Results show that the prediction errors induced by the ensemble forecast members whose initial errors are of the EOF\_1 + modes are the largest ones. Following this, we composite the initial errors corresponding to the EOF\_1 + mode and denote it as EP-Type initial errors. Fig. 10 present the structures of EP-Type initial ocean temperatures errors at different depth. It is shown that the EP-Type initial errors possess the ocean temperature patterns with positive anomalies over the upper layer of the central-eastern equatorial Pacific and negative anomalies in the lower layer of the western equatorial Pacific, plus the Subtropical North Pacific upper layers with a meridional dipolar mode and the Subtropical Southeast Pacific upper layers with meridional negative anomalies mode.

As demonstrated above, EP-Type initial errors could induce the significant SPB, especially the large prediction errors in the Niño3 area. In order to address the growth dynamical behaviors of EP-Type initial errors, Fig. 11 show a composite of the evolution of the prediction errors caused by EP-Type initial errors, and present the major mode of their evolutions respectively. The results illustrate that in the tropical Pacific, EP-Type initial errors often present the evolving mode initially similar to an El Niño decaying phase, and then present a transition to a cold phase, finally evolving into a mature La Nina-like mode. That is, the EP-type initial error evolves like a La Niña event and triggers a cold bias of prediction in central-eastern equatorial Pacific at leading 12 months.

Specially, the positive SSTA initial errors are confined to the central-eastern equatorial Pacific, and a weak westerly anomaly occurs only over the central tropical Pacific (Fig. 11). Under these conditions, the Bjerknes feedback process fails to establish. However, the large negative subsurface temperature anomalies lift the thermocline of the western equatorial Pacific and generate upwelling Kelvin waves. At the same time, the negative subsurface temperature anomalies propagate eastward. During the propagating process, they carry large cold water with them and cause a negative SSTA in the eastern Pacific. Meanwhile, the anomalous meridional mode structure in the Subtropical Southeast Pacific leads to the anomalous wind and then induce the anomalous latent heat release, thus cause the cold SST footprints moving toward central-eastern equatorial Pacific and strengthen the anomalous easterlies in the equatorial Pacific. Besides, the VM-like ocean temperature structure over the subtropical North Pacific could induce the warm SST footprints moving toward central equatorial Pacific, and it causes a positive SSTA and hence causes the initial negative SSTA errors in the equatorial Pacific to weaken. Therefore, the feedback from the Subtropical North Pacific is the negative feedback and competes with the other two feedback processes respectively from the western equatorial Pacific and the Subtropical Southeast Pacific. Finally, the fluctuation process from the lower layer of the western equatorial Pacific and the W-E-S feedback mechanism from the Subtropical Southeast Pacific play the dominant roles and causes the negative SSTA errors to be further amplified, ultimately evolving into a La Niña mode and yielding negative prediction errors for the EP-El Niño events. Therefore, for the EP-Type initial errors, the resultant negative prediction errors in Niño3 area originate from the lower layers of the western equatorial Pacific and the meridional negative anomalies mode in the upper layers of the subtropical southeast Pacific.

### 5. The determination of most sensitive initial error modes modulating intensities related to CP- and EP- El Niño

In Sections 4.1 and 4.2, we have revealed the patterns and evolving mechanism of the initial errors which induce the significant SPB, especially the largest prediction errors at the end of prediction time for the two types of El Niño events. The initial errors are CP-Type and EP-Type respectively and they mainly concentrated in a few regions with large anomalies. For CP-El Niño, the CP-Type initial ocean temperature errors are mainly located in the North Pacific upper layers with VM-like SSTA pattern (we denote it as region CP-Type-A, 20° N-60° N, 150° E-120° W, 0-85 m), and in the equatorial Pacific with positive anomalies in the lower layer of western Pacific. Such errors develop with a La Nina-like evolving mode and finally generate cold bias of SST in the central tropical Pacific at the 12-month lead time. The analysis of CP-Type errors evolution mechanism show that, the upper layers sea temperature errors of the North Pacific with VM-like structure tend to make CP-El Niño events underestimated in terms of amplitude and event to be predicted into a La Nina-like event but with cold center in the central tropical, which therefore mainly influences the amplitude of SST in the central Pacific associated with CP-El Niño. The above analysis implied that the intensity prediction of CP-El Niño events is more sensitive to the initial sea temperature errors in the North Pacific upper layers with VM-like SSTA pattern. For EP-El Niño events, the

EP-Type initial errors possess the ocean temperature patterns with positive anomalies over the upper layer of the central-eastern equatorial Pacific and negative anomalies in the lower layer of the western equatorial Pacific, plus the Subtropical North Pacific upper layers with a meridional dipolar mode and the Subtropical Southeast Pacific upper layers with meridional negative anomalies mode. Such errors finally develop into a canonical La Nina-like cooling mode with the cold center in the central-eastern equatorial Pacific at the 12-month lead time. The analysis of EP-Type errors evolution mechanism show that, the lower layers of the western equatorial Pacific and the meridional negative anomalies mode in the upper layers of the southeast Pacific (we denote it as region EP-Type-B, including 10°S-10°N, 130°E-135°W, 95–165 m and 15°S-30°S, 140°W-85°W, 0–85 m) tend to make EP-El Niño events underestimated in terms of amplitude and finally to be predicted into a La Nina-like event, which therefore cause large cold bias of SST in the equatorial central-eastern Pacific. The above analysis implied that the intensity prediction of EP-El Niño events is more sensitive to the initial sea temperature errors in these areas.

Associated with above analysis, we will ask that if identified CP-Type (or EP-Type) initial errors and their corresponding key mode errors in these above key areas are superimposed on CP-El Niño (or EP-El Niño), whether or not it may cause the large effect on the El Niño predictions? Furthermore, if additional observations are developed in these areas and then assimilated to the models, whether or not the large prediction errors of CP- and EP- El Niño may be reduced and even to be avoid? Firstly, to illustrate the validity of the identified key source areas of large prediction errors in reducing the prediction errors related to CP- and EP-El Niño events, we design one group of numerical experiments for CP-Type and EP-Type initial errors respectively. Based on the prediction results, we calculate the E-Niño3 and E-Niño4 to measure the amplitude errors of CP- and EP- El Niño events as followings:

$$\begin{aligned} E - \text{Niño3} &= \text{SSTA}^p(t)|_{\text{Niño3}} - \text{SSTA}^r(t)|_{\text{Niño3}}, \\ E - \text{Niño4} &= \text{SSTA}^p(t)|_{\text{Niño4}} - \text{SSTA}^r(t)|_{\text{Niño4}}, \end{aligned} \tag{3}$$

where,  $\text{SSTA}^p(t)|_{\text{Niño3}}$ (or  $\text{SSTA}^p(t)|_{\text{Niño4}}$ ) represents the predicted mean SSTA of Niño3 (or Niño4) regions.  $\text{SSTA}^r(t)|_{\text{Niño3}}$ (or  $\text{SSTA}^r(t)|_{\text{Niño4}}$ ) represents the Niño3 index (or Niño 4 index) of reference state EP-El Niño (or CP-El Niño). When the value of E – Niño3 (or E – Niño4) less than 0, it represents the prediction results caused by the initial errors underestimated the reference state EP-El Niño (or CP-El Niño events) in terms of amplitude. Also, to measure the benefit of data assimilation in the sensitive regions in reducing prediction errors for each type of El Niño events, we define the index RE to measure the reduction extent of the prediction errors in Eq. (4).

$$\text{RE} = (T'_{\text{whole-region}} - T'_{\text{remove-area}}) / T'_{\text{whole-region}} \times 100\%, \tag{4}$$

where  $T'_{\text{whole-region}}$  represents the prediction errors caused by CP-Type (or EP-Type) initial errors,  $T'_{\text{remove-area}}$  denotes the prediction errors caused by initial errors from sensitive areas or non-sensitive areas, indicating initial errors in sensitive areas or non-sensitive areas are eliminated.

In Section 2.2, we have selected eight “true state” CP-El Niño events and eight “true state” EP-El Niño events. In our strategy, the basic initial states with October (–1) and January (0) of each El Niño events are selected. Here, we make 3 groups of tests with the different new initial states and all the tests make the 1-year integration. The three groups of tests have the same basic initial states but with different initial errors. In order to classify the above three groups of tests, we make the Table 1 to provide the different groups of initial errors. Concretely, the three groups of tests are constructed as follows.

Firstly, for CP-El Niño, the new initial states are constructed by CP-Type initial errors superposed on the basic initial states with October (–1) and January (0) of each El Niño respectively, and then make the 1-year integration. We obtain a total of 16 predictions for CP-El Niño events. For EP-El Niño, as in CP-El Niño, but for EP-Type initial errors superposed on the initial states of each EP-El Niño event with October (–1) and January (0) and also make the 1-year integration. We also obtain a total of 16 predictions for EP-El Niño. We denote the test as CTL test.

Secondly, we retain CP-Type-A initial errors in CP-Type initial errors (or EP-Type-B initial errors in EP-Type initial errors) for CP-El Niño events (or EP-El Niño events), that’s, we eliminate initial errors beyond A pattern (B pattern) from CP-Type initial errors (EP-Type initial errors). Then we add the new initial errors on the initial values of each “true state” CP-El Niño events (or EP-El Niño events) and make the 1-year integration. The test is denoted as the Sen-I test.

Thirdly, CP-Type-A initial errors (or EP-Type-B initial errors) are removed from CP-Type initial errors (EP-Type initial errors) and the errors in other pattern beyond A (B) of CP-Type initial errors (EP-Type initial errors) are retained. With these updated initial errors superposed on the initial value of each “true state” CP-El Niño events (or EP-El Niño events), we make 1-year integrations respectively. We denoted the test as the Sen-II test. Each group of sensitive tests include 16 predictions for CP-El Niño and 16 predictions for EP-El Niño predictions.

Fig. 12 (a) present average amplitude errors of Niño4 (left coordinate, blue bars) calculated by Eq. (3) and reduction extent RE of the prediction errors calculated by Eq. (4) (right coordinate, yellow bars) caused by CP-Type initial errors (CTL test), CP-Type-A initial errors (Sen-I test) and by eliminating CP-Type-A errors from CP-Type initial errors (Sen-II test), respectively. Fig. 12 (b) present

**Table 1**  
initial errors of different groups of tests.

CTL test	Sen-I test	Sen-II test
CP-Type (EP-Type) initial errors	CP-Type-A (EP-Type-B) initial errors	CP-Type (EP-Type) minus CP-Type-A (EP-Type-B) initial errors

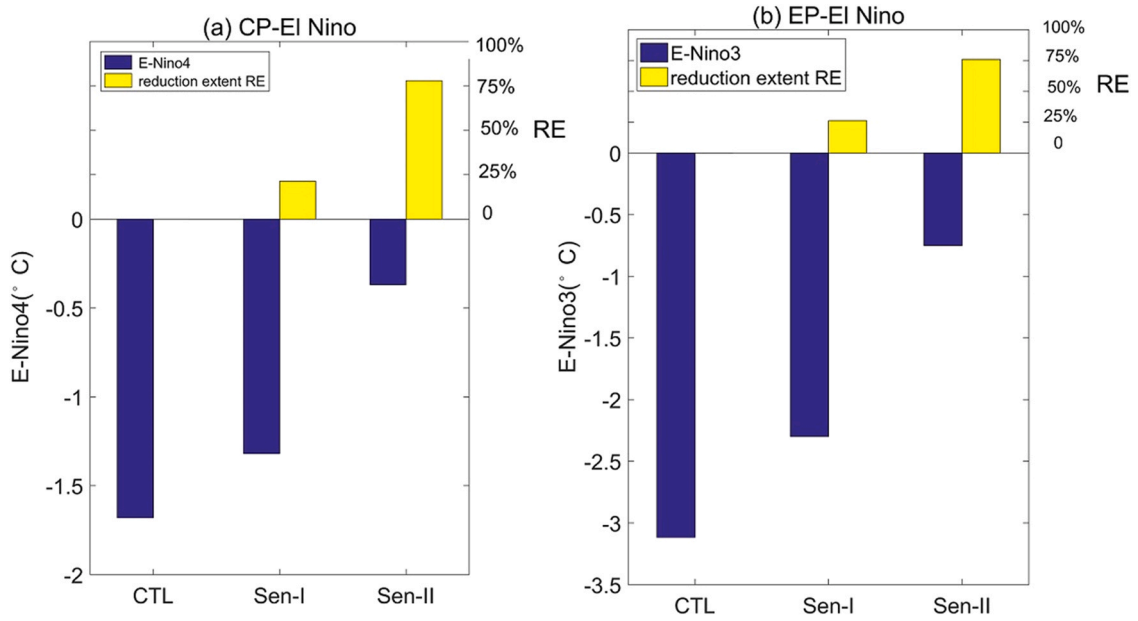


**Fig. 12.** The average amplitude errors of Niño4 (left coordinate, blue bars) and reduction extent RE of the prediction errors (right coordinate, yellow bars) caused by CTL test, Sen-I test and Sen-II test respectively with (a) CP-El Niño events and (b) EP-El Niño events.

average amplitude errors of Niño3 (i.e., E-Niño3, left coordinate, blue bars) and reduction extent RE of the prediction errors (right coordinate, yellow bars) caused by EP-Type initial errors (CTL test), EP-Type-B initial errors (Sen-I test) and by eliminating EP-Type-B errors from EP-Type initial errors (Sen-II test), respectively.

The sensitive experiments demonstrate that, for CP-El Niño, there exists large prediction errors of Niño4 areas when we add CP-Type initial errors and CP-Type-A initial errors on the initial value of each “true state” CP-El Niño events. While when we eliminate CP-Type-A initial errors from CP-Type initial errors, its corresponding absolute value of the prediction errors of Niño-4 SSTA (i.e., E-Niño4) is less than 0.5, and the subsequently reduction extent of the prediction errors can reach 77.98%, while the reduction extent of the prediction errors is only 23.6% when we retain CP-Type-A initial errors but eliminating initial errors in other regions. To put it another way, we can say that, CP-Type-A initial errors could modulate the intensity of CP-El Niño events and when we implement additional observations in the region, the large prediction errors of CP-El Niño event can be reduced effectively. For EP-El Niño, there also exists large prediction errors of Niño3 areas when we add EP-Type initial errors and EP-Type-B initial errors on the initial value of each “true state” EP-El Niño events. While when we eliminate EP-Type-B initial errors from EP-Type initial errors, its corresponding absolute value of the prediction errors of Niño-3 SSTA (i.e., E-Niño3) is far less than that of other two tests, and the subsequently reduction extent of the prediction errors can reach 75.96% compared with the reduction extent of the prediction errors only 13% for Sen-I test. To put it another way, we can say that, EP-Type-B initial errors could modulate the intensity of EP-El Niño events and when we implement additional observations in the region, the large prediction errors of EP-El Niño event can be reduced effectively.

From above discussion, we emphasize that the initial sea temperature accuracy in the Victoria mode (VM) region in the North Pacific is more important for better predictions of the intensity of the CP-El Niño than other regions in the Pacific. Also, the subsurface layer of the west equatorial Pacific and the surface layer of southeast Pacific are more important for better predictions of the intensity of the EP-El Niño than other regions in the Pacific. It is therefore clear that, in order to improve the accuracy of intensity prediction related to CP- and EP- El Niño events, we should mainly focus on initial sea temperature accuracy in not only the subsurface layer of the west equatorial Pacific but also the surface layer of southeast Pacific and the region covered by the VM-like mode in the North Pacific.

## 6. Summary and discussion

In this study, we investigated the two types of El Niño events simulated by GFDL-CM2p1 model and its “spring predictability barrier” (SPB) associations. By conducting the ensemble hindcast experiments related to the sea temperature on the whole Pacific and tracing the evolution of errors, results indicated that the prediction errors tend to experience their largest growth rate in spring and/or summer (MJJ and/or JJA) and exhibit a significant season-dependent evolution, generating a significant SPB for both the two types of El Niño events. However, compared with the EP-El Niño events, the relevant seasonal growth tendency level in spring and/or summer is much weaker for the CP-El Niño events; the prediction errors related to the CP-El Niño events at the end of the 12-month lead time are much smaller; the prediction members in CP-El Niño events which make a significant contribution to the SPB are less than that in EP-El Niño events. So, although there occurs the SPB phenomenon for the two types of El Niño events, there occurs the much weaker SPB phenomenon for CP- El Niño events.

Further analyses revealed that, for CP-El Niño events, CP-Type initial errors are identified which induce the significant SPB

especially the largest prediction errors in Niño 4 areas. The CP-Type initial errors consist of the subsurface temperature anomaly with the positive anomaly in the lower layers of the western equatorial Pacific and the upper layer sea temperature errors of the North Pacific with triple-like shape, referred to as the negative Victoria Mode (VM-). This type of initial errors evolve in a manner similar to the growth behavior of a La Niña event and cause a cold bias of SST with the cold center located at Niño4 area at leading 12 months. As for the EP-El Niño events, we also obtain one type of initial errors (denoted by EP-Type errors) that induce the significant SPB and especially the largest prediction errors in Niño3 areas. The EP-Type initial errors consist of the subsurface temperature anomaly with the negative anomaly in the lower layers of the western equatorial Pacific, the positive anomalies over the upper layers of the equatorial eastern Pacific, the meridional dipole pattern over the upper layer of the North Pacific plus the meridional negative pattern over the upper layer of the Subtropical Southeast Pacific. The EP-Type errors initially exhibit a rapid decay of an El Niño, and then a quick transition to a typical La Niña-like evolving mode with cold center in the east equatorial Pacific.

By conducting a series of sensitive experiments, we show that, when CP-Type-A errors are superimposed on CP-El Niño, it cause the large prediction errors. When CP-Type-A errors are eliminated from CP-Type initial errors, it causes the little prediction errors in Niño4 areas, and induces the largest reduction extent of the prediction errors. That's to say, the initial sea temperature errors of the North Pacific with triple-like shape, referred to as negative Victoria Mode (VM) induces the largest prediction errors in Niño4 areas and modulates the intensities of CP-El Niño events. For EP-El Niño events, when EP-Type-B errors are superimposed on EP-El Niño, it causes the large prediction errors. When EP-Type-B errors are eliminated from EP-Type initial errors, it cause the little prediction errors in Niño3 areas and induces the largest reduction extent of the prediction errors. Therefore, we emphasize that, the initial sea temperature errors in the subsurface layer of the western equatorial Pacific and the upper layer of the Southeast Pacific (15°S-30°S) with the meridional mode induce the largest prediction errors in Niño3 areas and modulates the intensities of EP-El Niño events.

In the present study, our results stress that, the initial sea temperature accuracy in the Victoria mode (VM) region in the North Pacific is more important for better predictions of the intensity of the CP-El Niño than other regions in the Pacific. Also, the subsurface layer of the west equatorial Pacific and the surface layer of southeast Pacific is more important for better predictions of the intensity of the EP-El Niño than other regions in the Pacific. Therefore, in order to reduce final prediction errors and obtain better predictions in terms of intensity on the two types of El Niño events, we should mainly focus on initial sea temperature accuracy in not only the subsurface layer of the west equatorial Pacific but also the surface layer of southeast Pacific and the region covered by the VM-like mode in the North Pacific. However, the prediction uncertainty related to the two types of El Niño events include not only the intensity prediction uncertainty but also the spatial structures prediction uncertainty. Especially, the CP-El Niño events are often predicted into EP-El Niño events. It may imply that, there also exists large prediction uncertainty in forecasting spatial structures of CP- and EP- El Niño events. So, whether or not the most sensitive initial error modes modulating intensities related to CP- and EP- El Niño can modulate the structure of the event? If not, what kind of initial errors can modulate the structure of CP- and EP- El Niño events furthest? When concerning both the intensity and structure predictions of CP- and EP- El Niño events, what's the most sensitive initial error modes? These issues all need to be considered and further studied in the future.

### CRedit authorship contribution statement

We declare that all authors have seen and approved the final version of the manuscript being submitted. Also, we warrant that the manuscript entitled "The most sensitive initial error modes modulating intensities of CP- and EP- El Niño events" is original, has not been published before and is not currently being considered for publication elsewhere.

### Declaration of Competing Interest

The authors declare that they have no known competing financial interests or personal relationships that could have appeared to influence the work reported in this paper.

### Acknowledgments

This work was jointly sponsored by the National Natural Science Foundation of China (Grant Nos. 41906022, 41930971, 41690124).

### References

- AchutaRao, K., Sperber, K.R., 2002. Simulation of the El Niño Southern oscillation: results from the coupled model intercomparison project. *Clim. Dyn.* 19, 191–209.
- Ashok, K., Behera, S.K., Rao, S.A., Weng, H.Y., Yamagata, T., 2007. El Niño Modoki and its possible teleconnection. *J. Geophys. Res.* 112, C11007.
- Bellenger, H., Guilyardi, E., Leloup, J., Lengaigne, M., Vialard, J., 2014. ENSO representation in climate models: from CMIP3 to CMIP5. *Clim. Dyn.* 42, 1999–2018.
- Bond, N.A., Overland, J.E., Spillane, M., Stabeno, P., 2003. Recent shifts in the state of the North Pacific: recent shifts in the state of the North Pacific. *Geophys. Res. Lett.* 30 (23) <https://doi.org/10.1029/2003GL018597>.
- Chen, G., Tam, C.Y., 2010. Different impacts of two kinds of Pacific Ocean warming on tropical cyclone frequency over the western North Pacific: impacts of ocean warming on TC frequency. *Geophys. Res. Lett.* 37 (L01803).
- Chen, M., Yu, J.Y., Wang, X., Jiang, W., 2019. The changing impact mechanisms of a diverse El Niño on the Western Pacific Subtropical High. *Geophys. Res. Lett.* 46, 953–962.
- Delworth, T.L., Broccoli, A.J., Rosati, A., Stouffer, R.J., Balaji, V., Beesley, J.A., Cooke, W.F., Dixon, K.W., Dunne, J., Dunne, K.A., Durachta, J.W., Findell, K.L., Ginoux, P., Gnanadesikan, A., Gordon, C.T., Griffies, S.M., Gudgel, R., Harrison, M.J., Held, I.M., Hemler, R.S., Horowitz, L.W., Klein, S.A., Knutson, T.R., Kushner, P.J., Langenhorst, A.R., Lee, H.C., Lin, S.J., Lu, J., Malyshev, S.L., Milly, P.C.D., Ramaswamy, V., Russell, J., Schwarzkopf, M.D., Shevliakova, E.,

- Sirutis, J.J., Spelman, M.J., Stern, W.F., Winton, M., Wittenberg, A.T., Wyman, B., Zeng, F., Zhang, R., 2006. GFDL's CM2 global coupled climate models. Part I: formulation and simulation characteristics. *J. Clim.* 19, 643–674.
- Ding, R.Q., Li, J.P., Tseng, Y., 2015. The impact of South Pacific extratropical forcing on ENSO and comparisons with the North Pacific. *Clim. Dyn.* 44, 2017–2034.
- Duan, W.S., Hu, J.Y., 2016. The initial errors that induce a significant “spring predictability barrier” for El Niño events and their implications for target observation: results from an earth system model. *Clim. Dyn.* 46, 3599–3615.
- Duan, W., Liu, X., Zhu, K., Mu, M., 2009. Exploring the initial errors that cause a significant “spring predictability barrier” for El Niño events. *J. Geophys. Res.* 114, C04022 <https://doi.org/10.1029/2008JC004925>.
- Duan, W.S., Tian, B., Xu, H., 2014. Simulations of the two types of El Niño events by an optimal forcing vector approach. *Clim. Dyn.* 43, 1677–1692.
- Duan, W.S., Wei, C., 2012. The “spring predictability barrier” for ENSO predictions and its possible mechanism: results from a fully coupled model. *Int. J. Clim.* 33, 1280–1292.
- Fan, L., Liu, Q., Wang, C., Guo, F., 2017. Indian ocean dipole modes associated with different types of ENSO development. *J. Clim.* 30 (6), 2233–2249.
- Griffies SM. Elements of MOM4p1 (GFDL Ocean Group Tech. Rep. 6, 444 pp.). NOAA/Geophysical Fluid Dynamics Laboratory, 2009, retrieved from (<http://www.gfdl.noaa.gov/fms>).
- Ham, Y.G., Kug, J.S., 2012. How well do current climate models simulate the two types of El Niño? *Clim. Dyn.* 39, 383–398.
- He, S.S., Zhang, W.J., Qi, L., et al., 2015. Contrasting SST anomalies over the Indian Ocean between the two types of El Niño events during boreal autumn. *Acta Meteorol. Sin.* 73 (3), 515–528.
- Hou, M.Y., Duan, W.S., Zhi, X.F., 2019. Season-dependent predictability barrier for two types of El Niño revealed by an approach to data analysis for predictability. *Clim. Dyn.* 53, 5561–5581. <https://doi.org/10.1007/s00382-019-04888-w>.
- Kao, H.Y., Yu, J.Y., 2009. Contrasting eastern-Pacific and central-Pacific types of ENSO. *J. Clim.* 22, 615–632.
- Kim, S.T., Yu, J.Y., Kumar, A., Wang, H., 2012. Examination of the two types of ENSO in the NCEP CFS model and its extratropical associations. *Mon. Weather Rev.* 140 (6), 1908–1923.
- Kug, J.S., Choi, J., An, S.I., Jin, F.F., Wittenberg, A.T., 2010. Warm pool and cold tongue El Niño events as simulated by the GFDL 2.1 coupled GCM. *J. Clim.* 23, 1226–1239.
- Larkin, N.K., Harrison, D.E., 2005. On the definition of El Niño and associated seasonal average U. S. weather anomalies. *Geophys. Res. Lett.* 32, L13705 <https://doi.org/10.1029/2005GL022738>.
- Lau, K.M., Yang, S., 1996. The Asian monsoon and predictability of the tropical ocean-atmosphere system. *Q. J. R. Meteorol. Soc.* 122, 945–957.
- Lin, C.Y., Yu, J.Y., Hsu, H.H., 2015. CMIP5 model simulations of the Pacific meridional mode and its connection to the two types of ENSO. *Int. J. Climatol.* 35, 2352–2358.
- Marathe, S., Ashok, K., Swapna, P., Sabin, T., 2015. Revisiting El Niño Modoki. *Clim. Dyn.* 45, 3527–3545.
- Min, Q., Su, J., Zhang, R., 2017. Observation-based comparisons of the impacts of the meridional modes of the South and North Pacific on the ENSO. *J. Clim.* 30 (5), 1705–1720.
- Milly, P.C.D., Shmakin, A.B., 2002. Global modeling of land water and energy balances. Part I: the land dynamics (LaD) model. *J. Hydrometeorol.* 3 (3), 283–299.
- Mu, M., Duan, W.S., Wang, B., 2003. Conditional nonlinear optimal perturbation and its applications. *Nonlinear Process Geophys.* 10 (6), 493–501.
- Mu, M., Duan, W.S., Wang, B., 2007a. Season-dependent dynamics of nonlinear optimal error growth and El Niño-Southern Oscillation predictability in a theoretical model: EL NIÑO predictability dynamics. *J. Geophys. Res.* 112, D10113.
- Mu, M., Xu, H., Duan, W.S., 2007b. A kind of initial errors related to “spring predictability barrier” for El Niño events in Zebiak-Cane model. *Geophys. Res. Lett.* 34, L03709 <https://doi.org/10.1029/2006GL-27412>.
- Rasmusson, E.G., Carpenter, T.H., 1982. Variations in the tropical sea surface temperature and surface wind fields associated with the Southern Oscillation/El Niño. *Mon. Weather Rev.* 10, 354–384.
- Ren, H.L., Liu, Y., Zuo, J., et al., 2016. The new generation of ENSO prediction system in Beijing climate center and its prediction for the 2014/2016 super El Niño event. *Meteorol. Mon.* 42, 521–531. <https://doi.org/10.7519/j.issn.1000-0526.2016.05.001>.
- Sullivan, A., Luo, J.J., Hirst, A.C., Bi, D., Cai, W., He, J., 2016. Robust contribution of decadal anomalies to the frequency of central-Pacific El Niño. *Sci. Rep.* 6 (38540), 38540. <https://doi.org/10.1038/srep38540>.
- Tian, B., Duan, W.S., 2015. Comparison of the initial errors most likely to cause a spring predictability barrier for the two types of El Niño events. *Clim. Dyn.* <https://doi.org/10.1007/s00382-015-2870>.
- Tian, B., Duan, W.S., 2016. Comparison of the initial errors most likely to cause a spring predictability barrier for two types of El Niño events. *Clim. Dyn.* 47, 779–792. <https://doi.org/10.1007/s00382-015-2870>.
- Wang, X., Wang, C., 2014. Brain structural changes and their correlation with vascular disease in type 2 diabetes mellitus patients: a voxel-based morphometric study. *Neural Regen. Res.* 9, 1548–1556. <https://doi.org/10.1007/s00382-013-1711-2>.
- Wang, X., Chen, M., Wang, C., Yeh, S.W., Tan, W., 2019a. Evaluation of performance of CMIP5 models in simulating the North Pacific Oscillation and El Niño Modoki. *Clim. Dyn.* 52 (3), 1383–1394. <https://doi.org/10.1007/s00382-018-4196-1>.
- Wang, X., Guan, C., Huang, R.X., Tan, W., 2019b. The roles of tropical and subtropical wind stress anomalies in the El Niño Modoki onset. *Clim. Dyn.* 52 (11), 6585–6597. <https://doi.org/10.1007/s00382-018-4534-3>.
- Wang, Z.C., Han, L., Ding, R.Q., Li, J.P., 2021. Evaluation of the performance of CMIP5 and CMIP6 models in simulating the South Pacific Quadrupole-ENSO relationship. *Atmos. Ocean. Sci. Lett.* 14 (4) <https://doi.org/10.1016/j.aosl.2021.100057>.
- Wu, H.Y., Wu, Y., 2018. Possible impacts of El Niño events of different types and intensity on precipitation in the subsequent first rainy season in South China. *Chin. J. Atmos. Sci.* 42 (5), 1081–1095. <https://doi.org/10.3878/j.issn.1006-9895.1711.17178>.
- Webster, P.J., Yang, S., 1992. Monsoon and ENSO: selectively interactive systems. *Q. J. R. Met. Soc.* 118, 877–926.
- Weng, H.Y., Ashok, K., Behera, S.K., Rao, S.A., Yamagata, T., 2007. Impacts of recent El Niño Modoki on dry/wet conditions in the Pacific rim during boreal summer. *Clim. Dyn.* 29, 113–129.
- Yeh, S.W., Kug, J.S., Dewitte, B., Kwon, M.H., Kirtman, B., Jin, F.F., 2009. Recent changes in El Niño and its projection under global warming. *Nature* 461, 511–515.
- Yeh, S.W., Wang, X., Wang, C., Dewitte, B., 2015. On the relationship between the North Pacific climate variability and the central Pacific El Niño! *Clim.* 28, 663–677. <https://doi.org/10.1175/JCLI-D-14-00137.1>.
- Yu, J.Y., Kao, H.Y., 2007. Decadal changes of ENSO persistence barrier in SST and ocean heat content indices: 1958–2001. *J. Geophys. Res.* 112 (D13), 2006JD007654 <https://doi.org/10.1029/2006jd007654>.
- Yu, J.Y., Kao, H.Y., Lee, T., 2010. Subtropics-related interannual sea surface temperature variability in the central equatorial Pacific. *J. Clim.* 23 (11), 2869–2884.
- Yu, J.Y., Wang, X., Yang, S., Paek, H., Chen, M., 2017. Changing El Niño-Southern oscillation and associated climate extremes, book chapter in climate extremes: patterns and mechanisms. AGU Geophys. Monogr. Ser. 226, 3–38.
- Yu, Y.S., Duan, W.S., Xu, H., Mu, M., 2009. Dynamics of nonlinear error growth and season-dependent predictability of El Niño events in the Zebiak-Cane model. *Q. J. R. Meteorol. Soc.* 135, 2146–2160.
- Zhang, W., Wang, Y., Jin, F.F., Stuecker, M.F., Turner, A.G., 2015. Impact of different El Niño types on the El Niño/IOD relationship. *Geophys. Res. Lett.* 42, 8570–8576.
- Zheng, F., Yu, J.Y., 2017. Contrasting the skills and biases of deterministic predictions for the two types of El Niño. *Adv. Atmos. Sci.* 34 (12), 1395–1403.
- Zebiak, S.E., Cane, M.A., 1987. A model El Niño-Southern oscillation. *Mon. Weather Rev.* 115 (10), 2262–2278.
- Zhu, J.S., Kumar, A., Huang, B.H., 2015. The relationship between thermocline depth and SST anomalies in the eastern equatorial Pacific: seasonality and decadal variations. *Geophys. Res. Lett.* 42, 4507–4515. <https://doi.org/10.1002/2015GL064220>.
- Zhu, J.S., Kumar, A., Huang, B.H., Balmaseda, M.A., Hu, Z.Z., Marx, L., Kinter Iii, J.L., 2016. The role of off-equatorial surface temperature anomalies in the 2014 El Niño prediction. *Sci. Rep.* 6, 19677. <https://doi.org/10.1038/srep19677>.